Available online at www.sciencedirect.com
ScienceDirect
C. R. Mecanique 337 (2009) 406–414
COMPTES RENDUS MECANIQUE

Combustion for aerospace propulsion

Effect of multiperforated plates on the acoustic modes in combustors

Elsa Gullaud [a,*], Simon Mendez [b], Claude Sensiau [b], Franck Nicoud [c], Thierry Poinsot [d]

[a] *SNECMA Villaroche, 77550 Moissey-Cramayel, France*
[b] *CERFACS, CFD team, 42, avenue Coriolis, 31057 Toulouse, France*
[c] *Université Montpellier, France*
[d] *IMF Toulouse, France*

Available online 18 July 2009

Abstract

The analytical model derived by Howe assessing the acoustic effect of perforated plates has been implemented in a 3D Helmholtz solver. This solver allows one to compute the acoustic modes of industrial chambers taking into account the multiperforated plates present for the cooling of the walls. An academic test case consisting of two coaxial cylinders, with the inner one being perforated is used to validate the implementation in the general purpose AVSP code. This case is also used to show the effects of the presence of the plates. In particular, the sensitivity of the acoustic damping to the bias flow speed will be studied. A maximum absorption speed is shown, and the behaviour towards an infinite speed will be illustrated by the academic case. Computations are also conducted in the case of an industrial helicopter chamber. The value of the maximum absorption speed is discussed to explain why the modes are in fact not much absorbed by the perforated plates, and that the frequencies are the same as for walls. ***To cite this article: E. Gullaud et al., C. R. Mecanique 337 (2009).***

Résumé

Impact des plaques multiperforées sur l'acoustique dans les chambres de combution. Le modèle analytique de Howe évaluant l'impact des plaques multiperforées sous l'effet d'une onde acoustique a été intégré dans un solveur de Helmholtz 3D. Ce code ainsi modifié permet de calculer les modes de chambres industrielles tout en prenant en compte la présence des plaques multiperforées utiles pour le refroidissement des parois. Le cas académique de deux cylindres coaxiaux dont l'un est perforé est considéré pour valider l'implémentation du modèle dans le code AVSP. Ce premier cas est aussi l'occasion d'illustrer l'effet des plaques perforées sur l'acoustique et en particulier l'influence de la vitesse de l'air dans les trous. Une vitesse correspondant à une absorption maximale est mise en évidence. Le comportement à grande vitesse est aussi étudié. Des calculs sont ensuite effectués dans le cas d'une chambre d'hélicoptère. Le fait que les modes de cette chambre ne sont pas très impactés dans le cas d'une utilisation industrielle est expliqué par le fait que la vitesse maximale d'absorption est loin de celle réellement utilisée. ***Pour citer cet article : E. Gullaud et al., C. R. Mecanique 337 (2009).***

Keywords: Combustion; Acoustics; Multiperforated plates; Damping; Combustion instabilities

Mots-clés : Combustion ; Acoustique ; Plaques multiperforées ; Amortissement ; Instabilités de combustion

* Corresponding author.
E-mail addresses: elsa.gullaud@cerfacs.fr (E. Gullaud), smendez@stanford.edu (S. Mendez), sensiau@tum.de (C. Sensiau), franck.nicoud@univ-montp2.fr (F. Nicoud), Thierry.Poinsot@imft.fr (T. Poinsot).

1631-0721/$ – see front matter
doi:10.1016/j.crme.2009.06.020

1. Introduction

Multiperforated plates (MP) are widely used in the combustion chambers of turbofan engines to cool the walls of the chambers which are submitted to high temperatures [1]. These plates consist of submillimeter apertures, across which the mean pressure jump forces a cold jet through the holes, from the casing into the combustion chamber. The micro-jets then coalesce to form a cooling film. Due to the tiny diameter of the perforations, the holes cannot be meshed for numerical computations. It is therefore necessary to have a model to account for the impact of perforated plates. This problem was encountered when performing computational fluid dynamics calculations [2,3] but also when computing acoustic modes of a combustion chamber. Indeed, MP are known to have a damping effect on acoustics [4,5], which is enhanced by the presence of a mean bias flow [6]. Acoustic waves interact with the shear layer, creating a vortex breakdown at the rims of the apertures, which converts part of the acoustic energy into vortical energy.

Howe proposed a model for this phenomenon [5], which will be recalled in Section 2. This model provides the acoustic impedance of a multiperforated plate in the presence of an acoustic wave and is well adapted to be inserted in the Helmholtz solver. It was validated, showing good agreement with experiments [6]. Improvements of this model have been made to take into account the thickness of the plate [7] and the interaction between the apertures [8]. Studies of the parameters influencing the sound absorption have been conducted [6]. In the present study, the implementation of Howe's model in the Helmholtz solver AVSP [9,10] is presented. AVSP solves the eigenvalue problem related to the wave equation in the frequency domain, and is able to provide the acoustic modes of a combustion chamber. With the implementation of Howe's model, it is now possible to compute the acoustic modes of a chamber, taking into account the multiperforated plates. After a brief description of Howe's model in Section 2, the coding is validated by comparing AVSP results to the ones given by an analytic solution on an academic test case in Section 3. A study of the influence of the parameters is also conducted in this section. The computations are then performed in Section 4 on a real industrial chamber.

2. Howe's model in AVSP

Howe's approach is the most classical model used to represent the behaviour of a multiperforated plate with bias flow and submitted to an acoustical excitation. Let us consider an array of circular perforations of diameter $2a$, with an inter-orifice spacing d, through which a mean flow of speed U, parallel to the apertures axis is imposed (see Fig. 1). When an acoustic perturbation is imposed, Howe's model can represent the behaviour of a multiperforated plate under the following hypotheses [5]:

- The acoustic excitation is at a low frequency, so that the wavelength is much larger than the orifice radius;
- The flow has a high Reynolds number, the viscosity is then only dominant at the rims of the aperture leading to the shedding of vorticity;
- The Mach number of the mean flow is low, so that the flow is incompressible in the vicinity of the aperture;
- The plate is infinitely thin;
- The aperture spacing is high compared to the aperture radius, so that the interaction between the apertures is negligible.

Acoustic energy is converted into vortical energy, due to the vortex shedding occurring at the aperture rims.

The Rayleigh conductivity K_R [11] of the aperture, relating the harmonic volume flux $\hat{Q}$ to the acoustic pressure jump across the plate, is defined by

$$K_R = \frac{i\omega\rho\hat{Q}}{\hat{p}^+ - \hat{p}^-} \tag{1}$$

where ρ is the mean density in the vicinity of the aperture, ω is the pulsation of the acoustic perturbation and $\hat{p}^+$ and $\hat{p}^-$ are the harmonic pressures upstream and downstream of the aperture respectively. We have

$$\hat{Q} = d^2\hat{u}^{\pm} \tag{2}$$

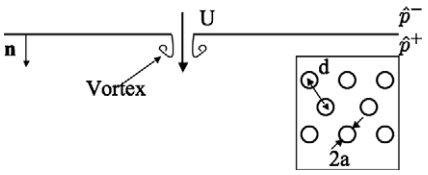

Fig. 1. Array of circular apertures, of diameter $2a$ and aperture spacing d, with a bias flow of speed U.

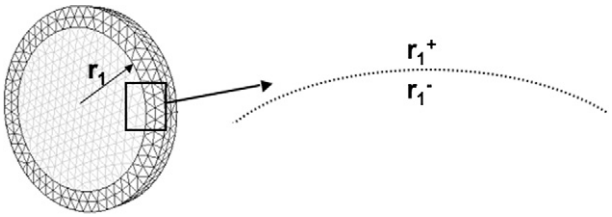

Fig. 2. Academic configuration: cylinder of radius r_2, with a perforated plate at r_1.

where $\hat{u}^{\pm}$ is the acoustic velocity on the plate, equal on both sides. Hence,

$$K_R = \frac{i\omega\rho_0 d^2 \hat{u}^{\pm}}{\hat{p}^+ - \hat{p}^-} \tag{3}$$

Howe expresses the Rayleigh conductivity for a circular aperture in an infinitely thin plate [5] as:

$$K_R = 2a(\Gamma_R - i\Delta_R) \tag{4}$$

where

$$\Gamma_R - i\Delta_R = 1 + \frac{\frac{\pi}{2} I_1(St) e^{-St} - i K_1(St)\sinh(St)}{St(\frac{\pi}{2} I_1(St) e^{-St} + i K_1(St)\cosh(St))} \tag{5}$$

St is the Strouhal number defined by $\omega a/U$. Using the momentum equation and Eq. (3), we obtain:

$$\nabla\hat{p}\cdot\mathbf{n} = \frac{K_R}{d^2}\left[\hat{p}^+ - \hat{p}^-\right] \tag{6}$$

Eq. (6) can be used as a Neumann boundary condition in the Helmholtz solver. The normal pressure gradient on each multiperforated boundary is expressed as a function of a, d, U, but non-linear in the pulsation ω. This non-linearity is handled by using an iterative method where a quadratic eigenvalue problem is solved at each sub-iteration in the code. Note that this procedure was developed initially to deal with complex valued boundary impedance in the Helmholtz solver [10].

3. Analytic validation

3.1. Analytics

First, an academic test configuration, for which an analytic solution can be derived, is presented. We consider the geometry depicted in Fig. 2. It consists of two coaxial cylinders, the inner one being perforated. The outer radius is r_2. The perforated plate is located at r_1. r_1^- and r_1^+ denote the upstream part of the plate and the downstream part respectively. Although the cylinder is 3D, the third dimension is considered small in regard to the others and so we will only consider radial and azimuthal modes, the longitudinal ones appearing at much higher frequencies.

Let us consider the wave equation written in the frequency domain [12].

The interior of the domain is denoted by Ω, and the boundary by $\delta\Omega$.

$$\begin{cases} \Delta\hat{p} + k^2\hat{p} = 0 & \text{on } \Omega \\ \nabla\hat{p}\cdot\mathbf{n} = 0 & \text{on } \delta\Omega \end{cases} \tag{7}$$

Considering $k^2 = k_r^2 + k_z^2$, Eq. (7) can be cast in polar coordinates (Eq. (8)), with $\hat{p} = R(r)\Theta(\theta)Z(z)$ [13].

$$\frac{1}{R}\frac{\mathrm{d}^2}{\mathrm{d}r^2}R + \frac{1}{rR}\frac{\mathrm{d}}{\mathrm{d}r}R + \frac{1}{r^2\Theta}\frac{\mathrm{d}^2}{\mathrm{d}^2\theta}\Theta + \frac{1}{Z}\frac{\mathrm{d}^2}{\mathrm{d}z}Z + \left(k_r^2 + k_z^2\right) = 0 \tag{8}$$

Since we only consider the radial and azimuthal modes, we have

$$\frac{1}{R}\frac{\mathrm{d}^2}{\mathrm{d}r^2}R + \frac{1}{rR}\frac{\mathrm{d}}{\mathrm{d}r}R + \frac{1}{r^2}\left(\frac{1}{\Theta}\frac{\mathrm{d}^2}{\mathrm{d}^2\theta}\Theta + n_\theta^2\right) + k_r^2 - \frac{n_\theta^2}{r^2} = 0 \tag{9}$$

In these conditions, the radial part of Eq. (8) can be reduced to a Bessel equation:

$$\left(\frac{\mathrm{d}^2}{\mathrm{d}r^2}R + \frac{1}{r}\frac{\mathrm{d}r}{\mathrm{d}r}R\right) + R \times \left(k_r^2 - \frac{n_\theta^2}{r^2}\right) = 0 \tag{10}$$

whose general solution is of the form:

$$R(r) = AJ_{n_\theta}(k_r r) + BN_{n_\theta}(k_r r) \tag{11}$$

where J_{n_θ} and N_{n_θ} are Bessel functions of the n_θ order. In the domain $r \leqslant r_1$, the pressure can be written:

$$R(r) = AJ_{n_\theta}(k_r r) \tag{12}$$

The Neumann function, which is singular in $r = 0$, is put aside. In the domain $r_1^+ \leqslant r \leqslant r_2$, solutions may be written:

$$R(r) = BJ_{n_\theta}(k_r r) + CN_{n_\theta}(k_r r) \tag{13}$$

A null acoustic speed is imposed on the outer cylinder. Applying the condition $\hat{u} = 0$ in $r = r_2$, we obtain:

$$BJ'_{n_\theta}(k_r r) + CN'_{n_\theta}(k_r r) = 0 \tag{14}$$

Jump conditions can also be written across the perforated plate:

$$\hat{p}\left(r = r_1^+\right) - \hat{p}\left(r = r_1^-\right) = \frac{i\omega\rho\, d^2}{K_R}\hat{u}\left(r = r_1^-\right) \tag{15}$$

$$\hat{p}\left(r = r_1^-\right) - \hat{p}\left(r = r_1^+\right) = -\frac{i\omega\rho d^2}{K_R}\hat{u}\left(r = r_1^+\right) \tag{16}$$

We then obtain the system

$$[M][X] = 0$$

where M is the matrix obtained by using Eq. (14), Eq. (15) and Eq. (16), and given by

$$\begin{bmatrix} 0 & J'_{n_\theta}(k_r r_2) & N'_{n_\theta}(k_r r_2) \\ \frac{d^2}{K_R}k_r J'_{n_\theta}(k_r r_1) + J_{n_\theta}(k_r r_1) & -J_{n_\theta}(k_r(r_1^+)) & -N_{n_\theta}(k_r(r_1^+)) \\ J_{n_\theta}(k_r r_1) & -J_{n_\theta}(k_r(r_1^+)) + \frac{d^2 k_r}{K_R}J'_{n_\theta}(k_r(r_1^+)) & -N_{n_\theta}(k_r(r_1^+)) + \frac{d^2 k_r}{K_R}N'_{n_\theta}(k_r r_2) \end{bmatrix}$$

and X is the vector

$$\begin{bmatrix} A \\ B \\ C \end{bmatrix}$$

Solving

$$\det(M) = 0 \tag{17}$$

releases the eigenvalues of the configuration.

Table 1
Comparison of the eigenfrequencies between AVSP and analytics.

	AVSP results with MP		Analytics with MP	
	Re(f)	Im(f) ($\mathcal{A}$%)	Re(f)	Im(f) ($\mathcal{A}$%)
$n_\theta = 1$	382.5 Hz	$-\mathbf{18.8}$ s^{-1} (26.7%)	382.56 Hz	$-\mathbf{18.9}$ s^{-1} (27.8%)
$n_\theta = 0$	534.1 Hz	$-\mathbf{97.5}$ s^{-1} (68.2%)	533.21 Hz	$-\mathbf{97.5}$ s^{-1} (68.3%)
$n_\theta = 2$	610.48 Hz	$-\mathbf{21.4}$ s^{-1} (19.8%)	611.04 Hz	$-\mathbf{21.64}$ s^{-1} (19.9%)

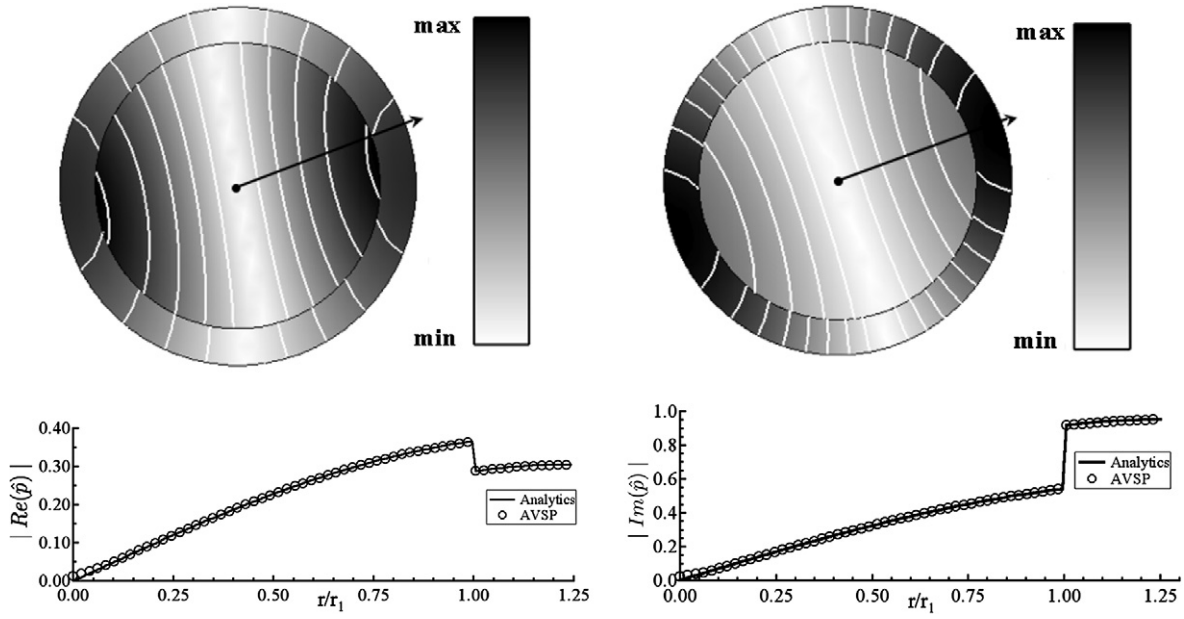

Fig. 3. First azimuthal mode: $n_\theta = 1$, Re(f) = 382.5 Hz, Im(f) = $-\mathbf{18.8}$ s^{-1}. Left: Re($\hat{p}$). Right: Im($\hat{p}$). Above: AVSP results. Below: Radial profiles of the real and imaginary part of $\hat{p}$ along the radius represented by the arrow (comparison analytics/AVSP).

3.2. Results

Let us consider the following parameters for the plate: $U = 5$ m/s, $a = 3$ mm and $d = 35$ mm, $r_1 = 0.2$ m and $r_2 = 0.25$ m. The configuration calculated in AVSP contains a tetrahedric mesh of 1186 nodes shown on Fig. 2. The sound speed is uniform and equal to 347 m/s. The eigenfrequencies are gathered in Table 1 and compared to the analytical results obtained by solving Eq. (17). The first three modes are considered. AVSP provides a complex frequency Re(f) + i Im(f) where Re(f) consists of the frequency of the mode, and Im(f) expresses the amplification rate of the mode. With the adopted convention $p'(x,t) = \mathrm{Re}\,5(\hat{p}(x)e^{-i\omega t})$, the ratio between the value of the pressure fluctuation at $t = 0$ and $t = T$ is given by Eq. (18).

$$\frac{|p'(x,t=T)|}{|p'(x,t=0)|} = \left|e^{\mathrm{Im}(\omega)T}\right| \tag{18}$$

Hence, the attenuation factor $\mathcal{A}$ in percent at a period T is given by $100[1 - |e^{2\pi \frac{\mathrm{Im}(f)}{\mathrm{Re}(f)}}|]$.

As expected, the eigenfrequencies have a negative imaginary part, which means the pressure fluctuation is damped. AVSP results are in good accordance with the theory. Figs. 3 and 4 show the radial profiles of the real and imaginary parts of $\hat{p}$ given by AVSP for the first and second modes. Analytic solutions are also given for comparison. Again, a good accordance is found. Note that the pressure jump across the perforated plate is visible on the real and imaginary parts of the harmonic pressure fluctuations, as well as on the isolines for the first azimuthal mode (Fig. 3). This comparison is conducted for a fixed bias flow speed (5 m/s), but Fig. 5 also shows good accordance between AVSP and analytical results for various bias flow speeds.

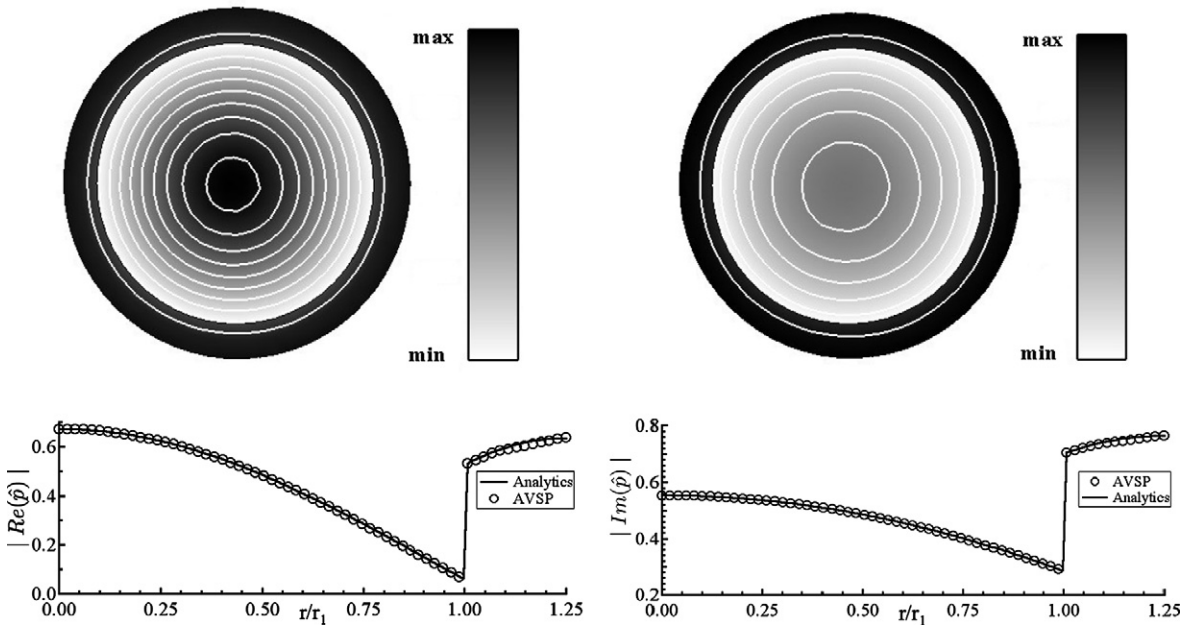

Fig. 4. Radial mode: $n_\theta = 0$, $\mathrm{Re}(f) = 534.1$ Hz, $\mathrm{Im}(f) = -\mathbf{97.5}\ \mathrm{s}^{-1}$. Left: $\mathrm{Re}(\hat{p})$. Right: $\mathrm{Im}(\hat{p})$. Above: AVSP results. Below: Radial profiles of the real and imaginary part of $\hat{p}$ (comparison analytics/AVSP).

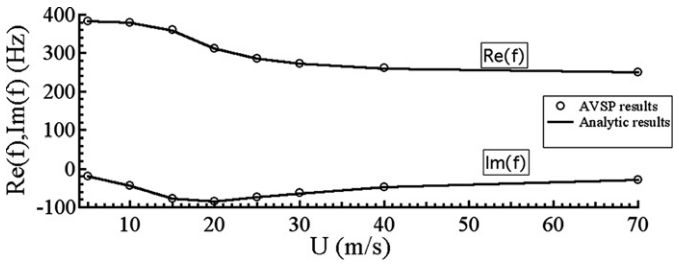

Fig. 5. Comparison between AVSP frequencies and analytics, for various speeds.

3.3. Study of the influence of the parameters

The impact of MP is further analysed in this section by comparing the results of four runs in Table 2.

- No plate: the inner cylinder is removed;
- Wall: the inner cylinder is replaced by a impermeable solid wall.
- MP5: the MP inner cylinder is present and the bias flow speed is $U = 5$ m/s;
- MP120: the MP inner cylinder is present and the bias flow speed is $U = 120$ m/s.

No damping occurs in absence of a MP: $\mathrm{Im}(f) = 0$ for the cases "wall" and "no plate". The influence of the mean bias flow speed on the damping is investigated at a fixed porosity ($\sigma = \pi a^2/d^2$). Table 2 shows the comparison of the first azimuthal mode ($n_\theta = 1$), at low bias flow speed (5 m/s) and at a high bias flow speed (120 m/s). The MP has a strong influence on the frequency. Fig. 6 shows that not only the frequency tends to the frequency of a wall at a high bias flow speed but also the structure of the mode does. Isolines of the harmonic pressure fluctuations are also plotted for a better understanding of the mode structure.

Fig. 7 shows the evolution of the damping in percent generated by the plate, when the bias flow speed changes between 5 m/s and 120 m/s. As previously shown by Hughes and Dowling [6], a speed optimizing the absorption is found. For the plate with a 3 mm radius perforation and a 35 mm inter-orifice distance ($\sigma = 2.3\%$), the jet speed

Table 2
Comparison of the first azimuthal mode, without MP, at low bias flow speed, at high bias flow speed, and with a wall. $\sigma = 2.3\%$.

No plate		MP5, $U = 5$ m/s		MP120, $U = 120$ m/s		Walls	
Re(f)	Im(f)	Re(f)	Im(f) ($\mathcal{A}\%$)	Re(f)	Im(f) ($\mathcal{A}\%$)	Re(f)	Im(f)
406.5 Hz	0 s^{-1}	382.5 Hz	-18.8 s^{-1} (26.7)	247.9 Hz	-16.8 s^{-1} (34.7)	246.5 s^{-1}	0 s^{-1}

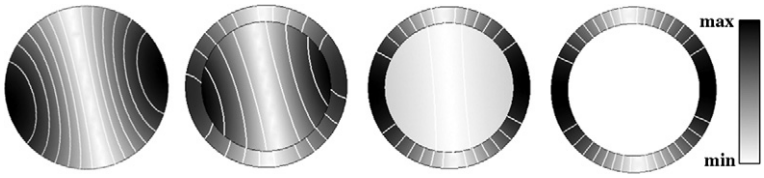

Fig. 6. Evolution of the first mode, without plate, at low (MP5: $f = 382.5$ Hz, $\mathcal{A} = 26.7\%$) and high bias flow speed (MP120: $f = 247.9$ Hz, $\mathcal{A} = 34.7\%$), and with a wall ($f = 246.5$ Hz, $\mathcal{A} = 0\%$).

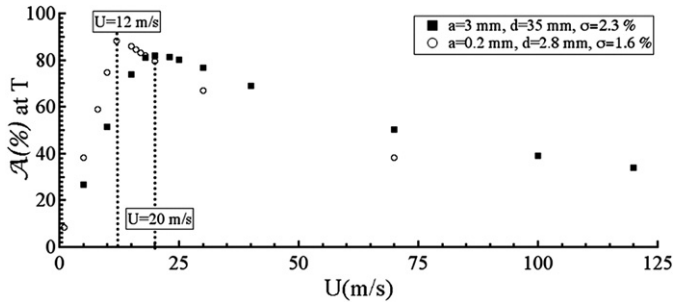

Fig. 7. Evolution of the damping as a function of the bias flow speed U, σ fixed.

corresponding to the maximum absorption is 20 m/s. Above this value, the damping drops. Another set of parameters is tested here ($\sigma = 1.6\%$) for which the maximum absorption speed is 12 m/s. This will be discussed in Section 4.

4. Computations on an industrial helicopter chamber

Computations are now conducted with AVSP in the case of an actual industrial chamber. This helicopter chamber is a reverse-flow annular chamber fueled by 15 injectors and is equipped with MP for cooling purpose, allowing the fresh air coming from the casing into the chamber to cool the walls. The computational domain is limited here to a 24°section, corresponding to one injector (Fig. 8). It contains the combustion chamber, the casing and the swirler. The influence of the geometry on the acoustics of this chamber was previously studied [14] and many computational fluid dynamics calculations were conducted [15,16]. The purpose here is to study the influence of the MP on the acoustics of the chamber. The locations of the MP are given in Fig. 8. The sound speed field is deduced from a previous LES[1] computation [17] (Fig. 9).

A unstructured mesh of 36 445 nodes is used in AVSP. Since we only consider a section of the chamber, only longitudinal modes will here be studied. The bias flow speed is calculated from the LES data and the geometrical characteristics of each plate.

4.1. Results

To assess the impact of MP in this chamber, we use a reference case when walls are used in place of the MP. Table 3 gives the eigenmodes for the computation with walls and MP. Frequencies are very close. The damping on the first eigenmode is very low (6.7% per period).

[1] Large Eddy Simulation.

Table 3
Comparison of the first two eigenfrequencies corresponding to the first two longitudinal modes, with walls, and with MP.

Walls		MP	
Re(f)	Im(f) ($\mathcal{A}$%)	Re(f)	Im(f) ($\mathcal{A}$%)
506.4 Hz	**0** s^{-1} (0%)	507.04	**−5.60** s^{-1} (6.7%)
1105.4 Hz	**0** s^{-1} (0%)	1118.7 Hz	**−61.54** s^{-1} (29.2%)

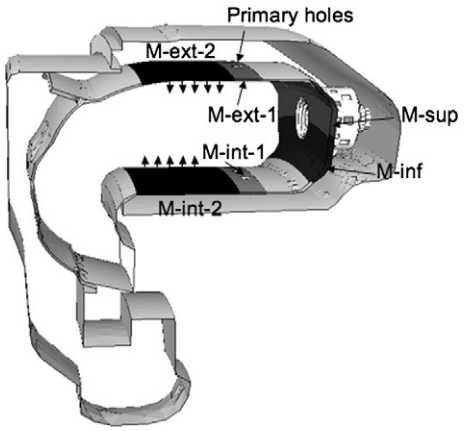

Fig. 8. Location of the MP on the chamber.

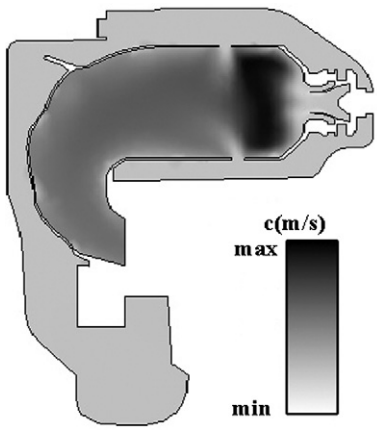

Fig. 9. Sound speed field.

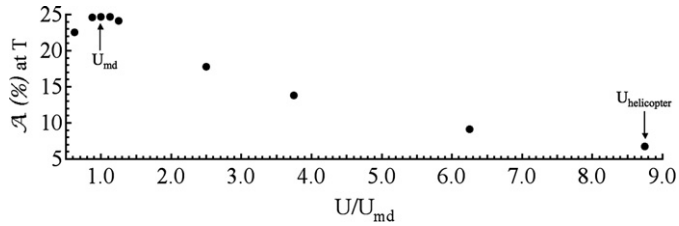

Fig. 10. Evolution of the damping of the first mode at 506.4 Hz in a period as a function of U/U_{md}.

For a better understanding of this low impact of the MP of the modes on this chamber, we are looking for the maximum absorption speed, for a fixed porosity. In Fig. 7, the set of parameters corresponding to the porosity of the chamber studied here was taken on the cylinder case, and the maximum absorption speed turned out to be 12 m/s. The maximal absorption occurs here at U_{md} (Fig. 10), which is the same order of magnitude as for the cylinder. But still the difference is not negligible and shows that the full geometry must be accounted for to predict the maximum absorption speed. At $U = U_{md}$, the damping is 25% per period. But at the real bias flow speed of the regime considered here, the damping drops to 6.7% per period. Indeed, the speed U_{md} is in the domain where the frequencies tend to be the ones when there is a wall. This shows that acoustics and the cooling process are two decoupled phenomena. For the bias flow speed corresponding to the best cooling of the chamber walls, acoustics are not impacted. Indeed, the behaviour of the chamber is very close to the one when walls are in place of the plates (see Fig. 11). On this figure, the acoustic pressure fields (real part of the acoustic pressure fluctuation) and its isocontours are presented for two different regimes of MP and with a wall. At the maximum absorption speed, the pressure node is not in the same place in the casing and the pressure gradient diminishes in the swirler.

5. Conclusion

A model for the acoustic behaviour of perforated plates has been implemented in the Helmholtz solver AVSP. This tool allows one to take into account MP in computations of the acoustics of a chamber. AVSP predicts damped acoustic modes, in agreement with what could be expected with perforated plates. The frequencies given by the code

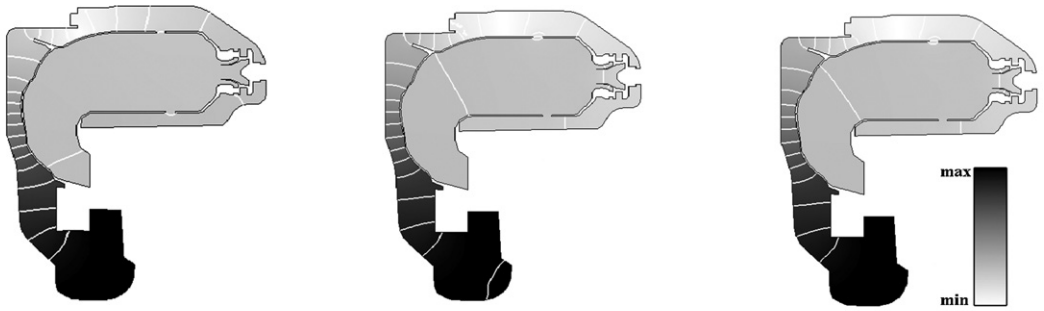

With MP, $U/U_{md} = 1$: $f = 530.9\ Hz$ $\mathcal{A} = 28.6\%$. With MP, $U/U_{md} = 8.75$: $f = 507.04\ Hz$ $\mathcal{A} = 6.7\%$ With walls: $f = 506.4\ Hz$ $\mathcal{A} = 0\%$.

Fig. 11. Spatial structure and isolines of $\hat{p}$ for the first mode.

have a negative imaginary part. But this damping strongly depends on both the parameters of the perforated plate and the bias flow speed. There exists a speed for which the damping reaches its maximum, and beyond this value, the perforated plate tends to behave like a wall and the damping drops. MP are used in industrial chambers in the purpose of cooling the chamber walls. They are not designed to have the best acoustic damping. It was found that with the geometrical characteristics of the perforated plates of the helicopter chamber considered here, and the flow rate injected in the perforations, the speed appears to be far above the maximum absorption speed. Therefore, the damping observed is low, and the frequencies of oscillations are not changed significantly. The cooling of the chamber is carried out without impacting on the chamber acoustics. However, with this tool, it is possible to know if by changing the regime of the cooling of the chambers, the acoustics will also get impacted.

Acknowledgements

The authors are grateful to the CINES (Centre informatique national pour l'enseignement supérieur) for the access to the supercomputer facilities.

References

[1] A.H. Lefebvre, Gas Turbines Combustion, Taylor & Francis, 1999.
[2] S. Mendez, F. Nicoud, Large-eddy simulation of a bi-periodic turbulent flow with effusion, Journal of Fluid Mechanics 598 (2008) 27–65.
[3] S. Mendez, F. Nicoud, Adiabatic homogeneous model for flow around a multiperforated plate, AIAA Journal 46 (10) (2008) 2623–2633.
[4] A. Cummings, Acoustics nonlinearities power losses at orifices, AIAA Journal 22 (6) (1983) 786–792.
[5] M.S. Howe, On the theory of unsteady high Reynolds number flow through a circular aperture, Proceedings of the Royal Society of London. Series A: Mathematical and Physical Sciences 366 (1725) (1979) 205–223.
[6] I.J. Hughes, A.P. Dowling, The absorption of sound by perforated linings, Journal of Fluid Mechanics 218 (1990) 299–335.
[7] X. Jing, X. Sun, Effect of plate thickness on impedance of perforated plates with bias flow, AIAA Journal 38 (9) (2000) 1573–1578.
[8] S.H. Lee, J.G. Ih, K.S. Peat, A model of acoustic impedance of perforated plates with bias flow considering the interaction effect, Journal of Sound and Vibration 303 (3–5) (2007) 741–752.
[9] L. Benoit, Prédiction des instabilités thermo-acoustiques dans les turbines à gaz, Ph.D. thesis, Université de Montpellier II, 2005.
[10] F. Nicoud, L. Benoit, C. Sensiau, Acoustic modes in combustors with complex impedances multidimensional active flames, AIAA Journal 45 (2007) 426–441.
[11] L. Rayleigh, The Theory of Sound, Mac Millan, 1894. Reprinted by Dover, New York, 1945.
[12] D.T. Blackstock, Fundamentals of Physical Acoustics, John Wiley & Sons, 2000.
[13] T. Poinsot, D. Veynante, Theoretical and Numerical Combustion, second ed., R.T. Edwards, 2005.
[14] C. Sensiau, Simulations numériques des instabilités thermoacoustiques dans les chambres de combustion aéronautiques, PhD thesis, Université de Montpellier II, 2008.
[15] G. Staffelbach, L.Y.M. Gicquel, G. Boudier, T. Poinsot, Large Eddy Simulation of self excited azimuthal modes in annular combustors, Proc. Combust. Inst. 32 (2) (2009) 2909–2916.
[16] G. Boudier, N. Lamarque, G. Staffelbach, L.M.Y. Gicquel, T. Poinsot, Thermo-acoustic stability of a helicopter gas turbine combustor using large-eddy simulations, International journal of Aeroacoustics 8 (1) (2009) 69–94.
[17] G. Millot, Simulation numérique d'écoulements en présence de plaques multiperforées: étude et validation d'un modèle homogène sous avbp, Technical report, Rapport confidentiel, 2008.